# Systematic investigation of acicular ferrite formation on laboratory scale

Denise **Loder**[1)] and Susanne Katharina **Michelic**[2)]

[1)] Chair of Ferrous Metallurgy, Montanuniversitaet Leoben, Austria, denise.loder@unileoben.ac.at

[2)] Chair of Ferrous Metallurgy, Montanuniversitaet Leoben, Austria, susanne.michelic@unileoben.ac.at

**Corresponding author:** Denise Loder

Postal Address: Franz-Josef-Straße 18, 8700 Leoben, Austria

Email: denise.loder@unileoben.ac.at

Phone: 0043/3842-402-2205

**Abstract**

By increasing the amount of acicular ferrite in the microstructure, steel toughness can be improved significantly. The steel composition, cooling rate, non-metallic inclusions and austenite grain size have a strong influence on the formation of acicular ferrite. The present paper describes and compares two approaches to study acicular ferrite formation in a titanium-deoxidized high-strength low-alloyed (HSLA) steel and its influencing factors on laboratory scale: route A simulates the formation of acicular ferrite after heat treatment; route B simulates the formation directly after solidification of the melt. The formation of acicular ferrite is essentially influenced by the former processing, which also changes the optimum cooling parameters substantially. $(Ti,Mn)_xO_y$ and $(Ti,Al,Mn)_xO_yS_z$ and are the predominant active inclusion types in the investigated steel.

**Keywords:** Acicular ferrite; Microstructure; Non-metallic inclusions; High temperature laser scanning confocal microscopy (HT-LSCM); HSLA steel

## 1. Introduction

In recent years, acicular ferrite (AF) has gained increasing importance for the production of high strength low alloyed (HSLA) steels. Providing excellent toughness and good weldability, acicular ferritic structures are no longer only the focus of

welding technology but are of increasing interest for steelmaking processes, following the concept of “oxide metallurgy”.[1] Acicular ferrite nucleates intragranularly at non-metallic inclusions (NMI), forming a chaotic structure of acicular and lenticular plates. These plates radiate from their point of nucleation in various directions, hindering the propagation of cleavage cracks in the material.[2–4]

Generally, two possibilities for the formation of acicular ferrite exist: First, by melting metallurgy, where acicular ferrite forms directly after solidification of the melt, or secondly, by heat treatment, where acicular ferrite forms after austenitization. In both cases, a specific adjustment and control of the steel cleanness in the melt is essential. The capability of non-metallic inclusions acting as active nuclei is strongly dependent on their chemical composition.[1,4–6] In a comprehensive review by Sarma et al.,[6] Ti- and Mn-containing inclusions are described as particularly active for acicular ferrite formation.

In previous studies, oxide powders or very small particles were added artificially to the steel melt to create the desired inclusion types, resulting in active nucleation sites for acicular ferrite.[7-10] In contrast, the present work only uses deoxidation and desulphurization products directly formed by reactions in the melt to provide the desired nucleation sites. With this approach, the inclusion content in the final product is not artificially increased by the addition of synthetic particles.

In addition to the non-metallic inclusions, the steel composition, the cooling rate and the austenite grain size are major influencing factors regarding the formation of acicular ferrite.[2,6,11–17] These four influencing factors interact strongly; already slight changes in one parameter can require the adjustment of the other factors.[6,18,19] The present work describes two different approaches on laboratory scale for the investigation of acicular ferrite formation. Both enable the systematic analysis of the main influencing factors and their coaction impact. The procedure, advantages and limitations of both approaches are discussed in detail.

## 2. Experimental methods

Within this paper, two different routes to study the acicular ferrite formation are presented and applied to a titanium deoxidized HSLA steel. The target steel composition for both routes as well as the final chemical compositions obtained after the experiment are shown in **Table 1**. *Route A* is a two-step process, including melting experiments in a Tammann type furnace and heat treatments by a High Temperature–Laser Scanning Confocal Microscope (HT-LSCM). *Route B* is a one-step process using dipping tests in a vacuum induction furnace. **Figure 1** schematically illustrates the procedures of the two approaches.

**Table 1:** Steel composition [wt.-%].

| | C | Mn | Si | Al | Ti | O | S | N |
|---|---|---|---|---|---|---|---|---|
| Target | 0.230 | 1.500 | | | 0.050 | | | 0.003 |
| Steel A | 0.230 | 1.480 | 0.017 | 0.005 | 0.050 | 0.007 | 0.007 | 0.005 |
| Steel B | 0.236 | 1.520 | 0.069 | 0.001 | 0.049 | 0.002 | 0.002 | 0.003 |

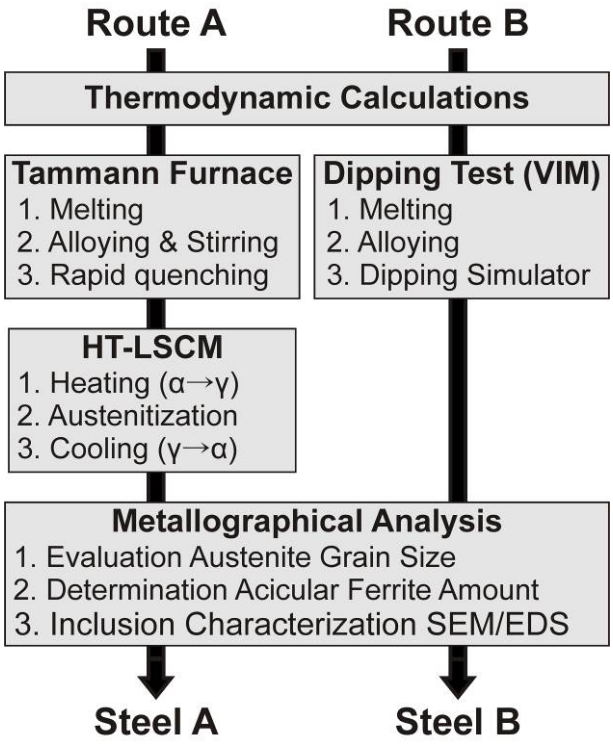


**Figure 1:** Flow chart of two different approaches for studying the acicular ferrite formation on laboratory scale.

Both routes start with thermodynamic calculations of the inclusion formation and modification. Therefor *FactSage 6.4* with the databases *FactPS, FToxid* and *FSstel* is used. Inclusion diagrams, which can be used to adjust a defined steel composition to form specific inclusions types, are created by the module *PhaseDiagram*: two elements are varied (x-/y-axes) and the stable inclusion phases at a defined temperature are plotted. The inclusion diagram for the steel composition used in this study is displayed in **Figure 2**. To study the influence of different inclusion types on the formation of acicular ferrite, an initial oxygen content of 300 ppm and an initial sulphur content of 70 ppm is chosen to produce stable $TiO_x$, MnS and ASlag inclusions. ASlag is a homogeneous mixture of oxidic and sulphidic inclusion phases, which is liquid at processing temperature. The determined steel composition is used as input data for a process model using the module *Equilib*. This model simulates the stepwise process of the melting experiments and the resulting changes in the inclusion landscape. A detailed description of the model as well as a comparison

between calculated and experimental results can be found in Ref. 20. Based on these thermodynamic calculations, the melting experiments are performed.

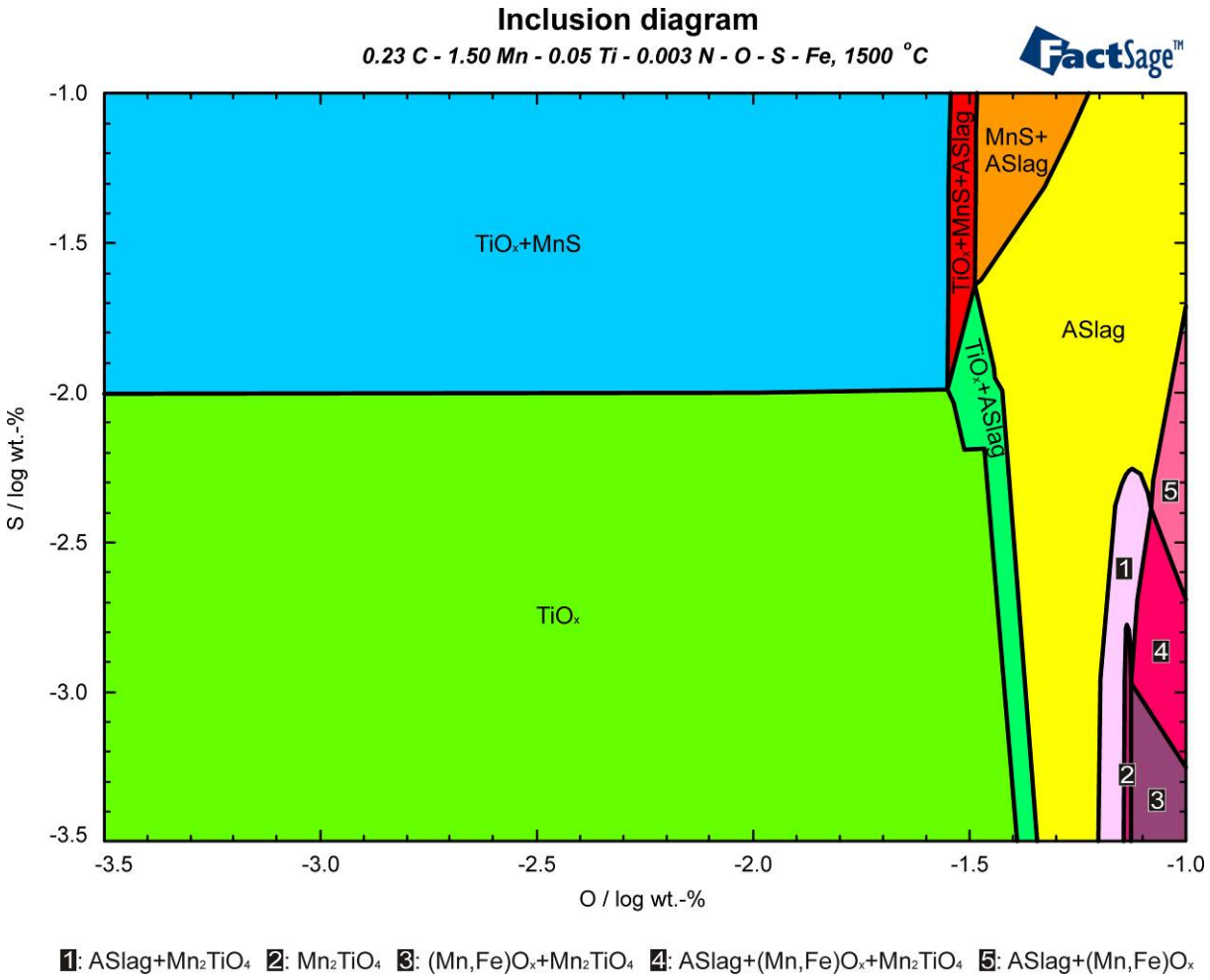


**Figure 2:** Inclusion diagram.

### 2.1. Route A

For route A, a Tammann type furnace (Ruhrstrat HRTK 32 Sond.) is used to produce material with a defined and homogeneously distributed inclusion landscape. The Tammann type furnace is an electric resistance furnace that can be heated to 1700 °C. A description of the Tammann type furnace and the used raw materials is given in Ref. 20-22. The relevant experimental steps are:

- Heating the unalloyed steel together with an oxygen rich pre-melt at 10 °C/min, resulting in a melt with an initial content of 300 ppm oxygen and 80 ppm sulfur.
- The melt is held for 19 min at the experimental temperature of 1600 °C. Carbon granules and electrolytic manganese are added after 6 min to obtain

0.230 wt.-% C and 1.500 wt.-% Mn. Thereby, the oxygen content of the melt is decreased to 140 ppm.

- The melt is deoxidized with titanium after 14 min, reaching a content of 0.050 wt.-% Ti.
- Special attention is paid to the stirring of the melt to ensure a homogenous inclusion distribution and to the rapid quenching to prevent inclusion flotation during solidification.

In route A, the described melting experiment is followed by heat treatment in the HT-LSCM. Therefore, the sample produced in the Tammann type furnace is cut into small pieces with a size of 5.0 x 5.0 x 1.2 mm. HT-LSCM enables the in situ observation of phase transitions in steel, such as the α→γ transformation and the formation of acicular ferrite. HT-LSCM helps to investigate the mechanism and the influencing factors of acicular ferrite formation. The HT-LSCM consists of a VL2000DX laser scanning confocal microscope, produced by Lasertec, an attached SVF17-SP high-temperature furnace and the associated hardware and software from Yonekura. To control the temperature during the experiment, a Pt-Rh thermocouple type S is installed in the furnace. A detailed description of the experimental set-up, as well as its function and advantages, can be found in Ref. 23-26. Before the experiment, the furnace chamber is repeatedly evacuated and flushed with argon 6.0 to ensure an inert furnace atmosphere. Additionally, the argon stream is purified in a gas-train and a Ti-getter furnace before entering the chamber to remove any residual oxygen. After heating to 1400 °C, the steel sample is austenitized for 100 s and then cooled to room temperature at varying cooling rates. In the present study, two cooling rates (A-1 and A-2) used in the HT-LSCM experiments are discussed; their profiles are shown in **Figure 3**. Cooling rate A-1 approximately corresponds to the continuous cooling of the dipping test in route B (cooling curve B-1). To characterize the cooling procedure, the cooling rate between 800 and 600 °C (Δ8/6) is used. The in-situ observed phase transitions during heating, austenitization and cooling in the HT-LSCM are displayed in **Figure 4**. A complete summary of all tested cooling rates in the HT-LSCM experiments and the results of these investigations are described in Ref. 27.

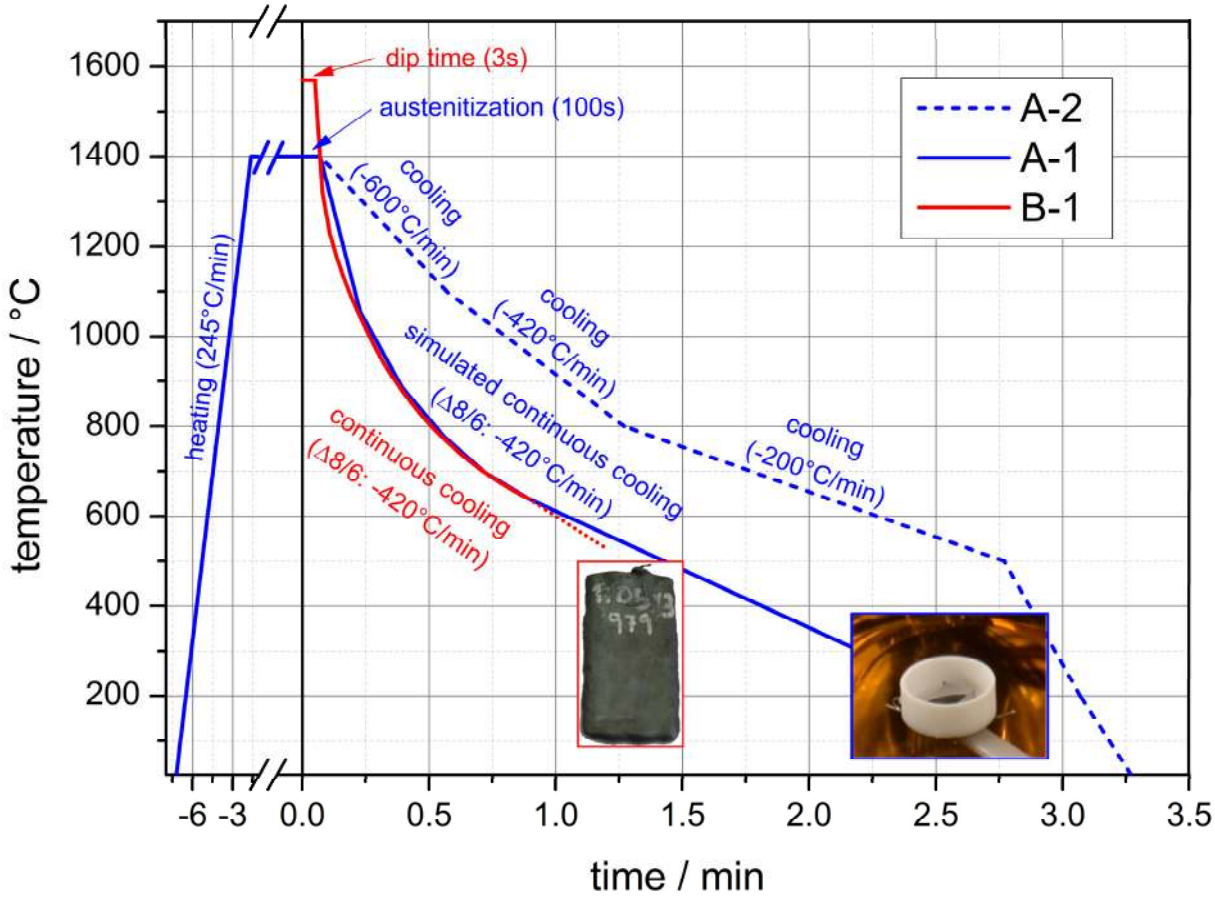


**Figure 3:** Temperature profiles of HT-LSCM experiments (Route A) and dipping test (Route B).

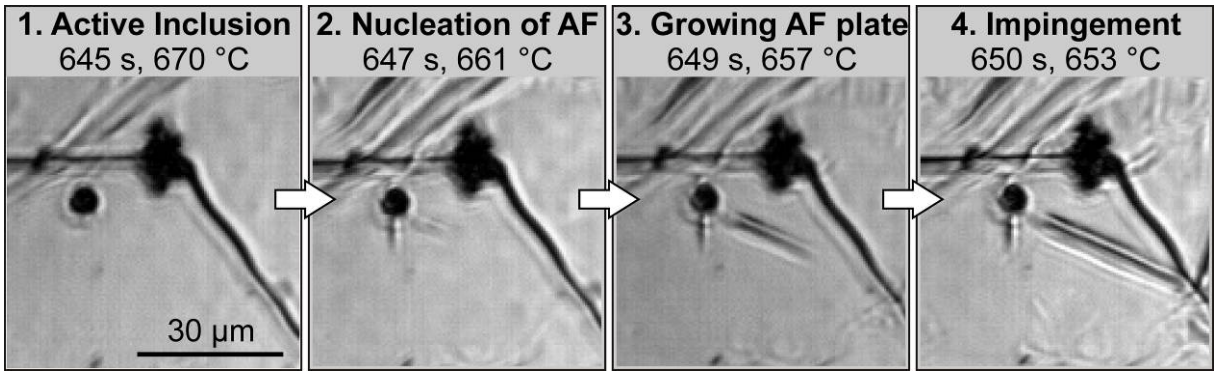


**Figure 4:** In situ observation of phase transitions in steel A during HT-LSCM treatment A-2.

### 2.2. Route B

In route B, a dipping test, originally applied to reproduce the solidification during strip casting,[28,29] is used to study the formation of acicular ferrite in the defined steel grade. For this purpose, a dipping test simulator, which is attached to a vacuum

induction-melting furnace (VIM), is applied. Due to the formation of acicular ferrite directly after solidification of the melt, this approach can also be applied for the investigation of acicular ferrite in welding, as confirmed previously by Vanovsek et al.[30] The experimental procedure is summarized as follows:

- A steel melt is built up under inert gas atmosphere inside the VIM with MgO-based refractory lining and is deoxidized with FeSi and FeTi.
- Dipping samples are taken by a test specimen consisting of a metallic substrate surrounded by ceramic fiber material. The specimen is mounted onto the linear adjustment of the dipping test simulator and is accelerated into the melt (melt temperature: 1570 °C). The specimen is held there for 3 s, and the liquid steel finally solidifies onto the metallic substrate. Further details of the dipping procedure are provided in Ref. 28-31.
- After reacceleration into the simulator chamber, the measurement of the surface temperature by a pyrometer is initiated. Simultaneously with every dipping sample, a tube sample is taken, which is used for chemical analysis.
- By varying the dip time, samples with different thicknesses can be produced. The cooling rate is strongly dependent on the sample thickness, so various cooling rates can be tested by changing the dip time. Different cooling systems, e.g., quenching in water, can be performed. The influence of various cooling rates on the formation of acicular ferrite in the dipping test has previously been investigated by the authors.[31] The latter work identified a dip time of 3 s and air cooling as the optimum for the analyzed steel grade concerning the adjustment of a possible high amount of acicular ferrite (see cooling curve B-1 in **Figure 3**).
- Using this setting, acicular ferrite can be produced directly after solidification. No additional heat treatment is necessary. Nevertheless, the examination of the produced dipping samples by HT-LSCM would be possible.

### 2.3. Metallographic analyses

Finally, steels A and B are investigated metallographically with respect to the austenite grain size, acicular ferrite amount and inclusion landscape:

- Due to the large impact of the austenite grain size on the formation of acicular ferrite, the determination of the prior austenite grain size is essential. Within the present work, a computerized routine using the image analysis software Clemex Vision 7.0 is applied. The routine calculates the austenite grain size distribution based on images taken by optical microscopy. Samples treated in the HT-LSCM are thermally etched and consequently do not require any further chemical etching. For all other analyses, etching with picric acid is performed. Detailed information on the evaluation routine and the necessary sample preparation is given in Ref. 27,32.
- To quantify the impact of the tested parameters, the fraction of acicular ferrite in the final microstructure is determined by a computerized method, shown in

**Figure 5** using steel A as an example. The method analyzes images from optical microscopy of Nital etched samples using the image analysis software Clemex Vision 7.0. A more detailed description of this procedure can be found in Ref. 32.

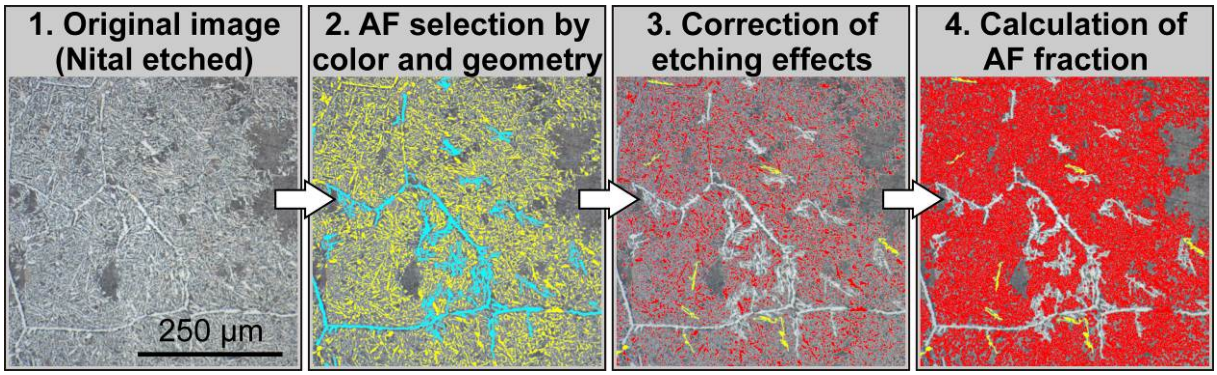


**Figure 5:** Computerized determination of the acicular ferrite fraction in steel A.

- Several types of non-metallic inclusions act as nuclei for acicular ferrite. Hence, the inclusion landscape, focusing on the determination of active inclusion types, must be evaluated. Inclusion characterization is performed by manual and automated SEM/EDS measurements using an FEI Quanta 200 MK2 scanning electron microscope (SEM), which is equipped with an energy dispersive X-ray spectrometer (EDS) system from Oxford Instruments. The function and advantages of the manual and automated SEM/EDS analysis are discussed in Ref. 33-35. The automated analyses are performed at an accelerating voltage of 15 kV and are limited to a minimum particle size of 1.1 µm ECD (Equivalent Circle Diameter). In route A, the analysis of the inclusion landscape is performed before heat treatment by HT-LSCM to obtain information about potential nuclei before the acicular ferrite formation starts. Route B is a single-step process, so inclusion characterization can only be performed after acicular ferrite formation. In both routes detailed studies of active inclusions are conducted after the experiments. For this purpose, slightly Nital etched samples are investigated by manual SEM/EDS. The necessary sample size for the manual analyses can be calculated by means of statistics (estimation of proportions based on the population known from the automated SEM/EDS results).

### 2.4. Comparison of route A and B

Based on the results of the metallographic analyses, the potential of the selected steel grade for acicular ferrite formation can be evaluated. Specific adjustment of the main influencing parameters enhancing the potential for acicular ferrite formation can be realized by both approaches. Depending on the factors of interest and the simulated production process, the more appropriate route can be chosen: route A

simulates a heat treatment process and provides excellent controllable conditions during the experiments due to the small-scaled system; route B is closely related to strip casting or welding processes and is a large-scaled laboratory experiment. Important key facts, which should be considered before determining the method of choice, are summarized in **Table 2**.

**Table 2:** Key facts of routes A and B for the study of acicular ferrite.

| | **Route A** | **Route B** |
|---|---|---|
| Production of samples | two-step process | one-step process |
| Simulated process | heat treatment | rapid solidification directly from the liquid |
| Process modelling | ++ | + |
| Melting furnace | Tammann furnace | VIM |
| Melt weight | ca. 100 g | ca. 20 kg |
| Sample weight | ca. 0.2 g | ca 90 g |
| Formation of NMI | by deoxidation/desulfurization (no addition of particles) | |
| Heat Treatment | HT-LSCM | - |
| Formation of AF | after austenitization | after solidification |

With both routes an accurate adjustment of the steel composition is possible, as displayed in **Table 1**. However, due to the necessary FeSi treatment in the VIM during route B, an increased silicon content is found in steel B. In contrast, the aluminum content is higher in steel A due to the use of an alumina crucible for the Tammann type furnace experiments. Additionally, the oxygen and sulphur contents are higher in steel A compared to steel B. A possible explanation for this difference can be the stronger bath movement and the longer processing time in the VIM (route B) enabling better conditions for inclusion separation than in the Tammann furnace (route A). Due to the lack of slag in the Tammann furnace, the possibility for inclusion separation is limited. A high number of inclusions can be helpful in laboratory experiments to study inclusions' influence on the acicular ferrite formation. But with respect to industrial processes, which generally require possibly low inclusion contents, route B is considered as more representative due to the improved conditions for inclusion separation. In contrast, due to the small-scaled system in route A and the well controllable experimental conditions, an undesired burn-off of elements can be mostly avoided.

In the melting experiments, non-metallic inclusions are formed by deoxidation and desulfurization; no particle powders are added artificially in either route A nor in route B. In route A, the steel melt is cast, and samples for HT-LSCM are cut out. Before HT-LSCM, the samples are analyzed with respect to their chemical

composition by single spark spectroscopy and LECO measurements as well as their inclusion landscape by automated SEM/EDS to ensure that the target steel composition was reached and the previously defined inclusion types favorable for acicular ferrite nucleation had formed. Due to the low melt weight and the easy handling of the Tammann type furnace, a wide range of different chemical compositions can be tested. In contrast, route B uses a higher melt weight and the handling of the furnace is more complex, so the amount of possible tests is limited. Because of the single-step process, all analyses in route B are performed at the end, and no information about the material is available before the acicular ferrite formation. However, route B plays an important role concerning industrial feasibility: the large-scaled experiment is essential for the possible industrial implementation.

During HT-LSCM treatment in route A, the temperature can be controlled very accurately, enabling a detailed study of the austenite grain size. In route B, the austenite grain size results from the selected dip time, and no further adjustment is possible. The precise temperature control in the HT-LSCM also allows for testing various cooling rates. In route B, the cooling rate can be varied by changing the dip time. But for each dip time, only one cooling curve is possible.

**Figure 6** illustrates the applicability of routes A and B for the different investigated parameters.

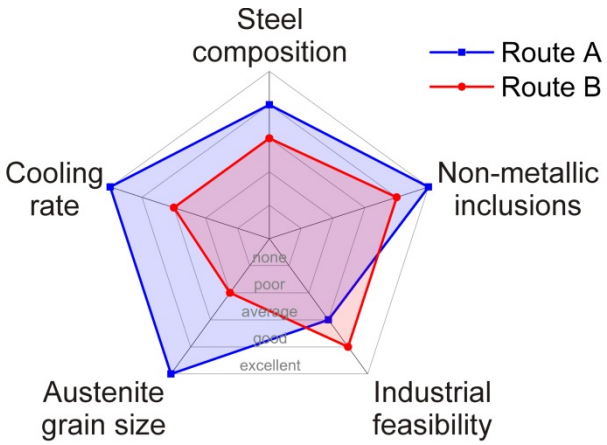


**Figure 6:** Applicability of routes A and B for the investigation of the main parameters.

## 3. Results and discussion

The produced samples are analyzed with respect to austenite grain size, acicular ferrite amount and inclusion landscape.

### 3.1. Austenite grain size

The prior austenite grain size is determined with approximately 210 µm in steel A and approximately 125 µm in steel B (see **Figure 7** and **Table 3**). Generally, it is well

accepted in literature [XY] that larger austenite grains promote the nucleation of acicular ferrite. For the heat-treatment in route A, austenitization temperature and holding time were adjusted at 1400 °C and 100 s, respectively, in order to enhance austenite grain growth. In route B, the austenite grain size can only be influenced by the dip time. However, the dip time also influences the cooling rate during the austenite-ferrite-transition. In the present study, the dip time is set with 3 s which proved to be the optimum for the cooling rate during phase transition but not for austenitization. Nevertheless, a change in dip time to create larger austenite grains would reduce the amount of acicular ferrite, as already found in previous investigations (see Ref. 31).

Additionally, another factor which influences the austenite grain size has to be taken into account: In steel B a high amount of TiN particles is present (see subsection 3.3), which reduces the austenite grain growth by pinning effects.

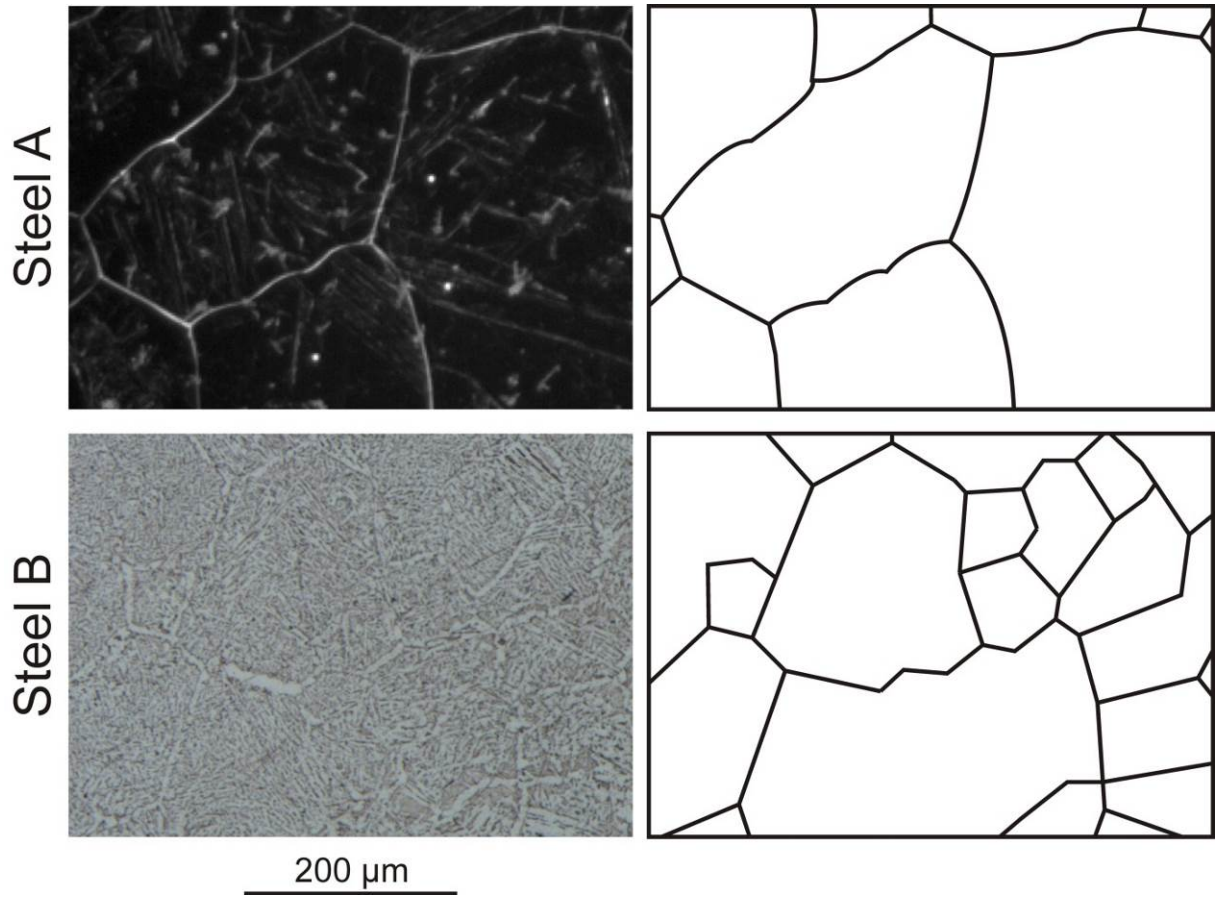


**Figure 7:** Austenite grains in steel A after heat treatment A-2 (thermally etched) and steel B after heat treatment B-1 (picric etched).

**Table 3:** Austenite grain size and AF-amount in steels A and B.

| | Method | Cooling curve | Austenite grain size/µm | AF amount/% |
|---|---|---|---|---|
| Steel A | HT-LSCM | A-2 | 210 | 72 |
| | | A-1 | | 11 |
| Steel B | Dipping test | B-1 | 125 | 80 |

### 3.2. Acicular ferrite

For both approaches, detailed studies of the cooling rate's influence on the amount of acicular ferrite were published previously.[27,31] In the present work, two different cooling rates, which are shown in **Figure 3**, are discussed. In route A, the maximum acicular ferrite amount of 72 % is achieved with cooling rate A-2; in route B, the highest acicular ferrite amount of 80 % is achieved when applying cooling rate B-1, which is significantly higher than A-2. (see **Table 3**). As shown in **Figure 8,** for both cooling rates A-2 and B-1 the final microstructure consists of perlite, grain boundary ferrite and Widmannstätten ferrite. Visible active inclusions for acicular ferrite are marked with white arrows.

It is important to mention, that applying comparable cooling rates in both routes (A-1 and B-1) leads to significant differences concerning the amount of acicular ferrite. Using cooling curve A-1 in the HT-LSCM only results in an acicular ferrite amount of 11 %, whereas a comparable cooling rate B-1 in the dipping tests resulted in 80 % acicular ferrite. Thus, if the two steels are cooled using a comparable cooling rate, the amount of acicular ferrite in steel A is significantly lower compared to steel B. Using the optimized cooling rate A-2, the acicular ferrite amount in steel A increases but does not reach the value of steel B, although the austenite grain size is significantly larger in steel A and should therefore promote acicular ferrite. These results prove the substantial influence of the former processing of the sample concerning the final microstructure.

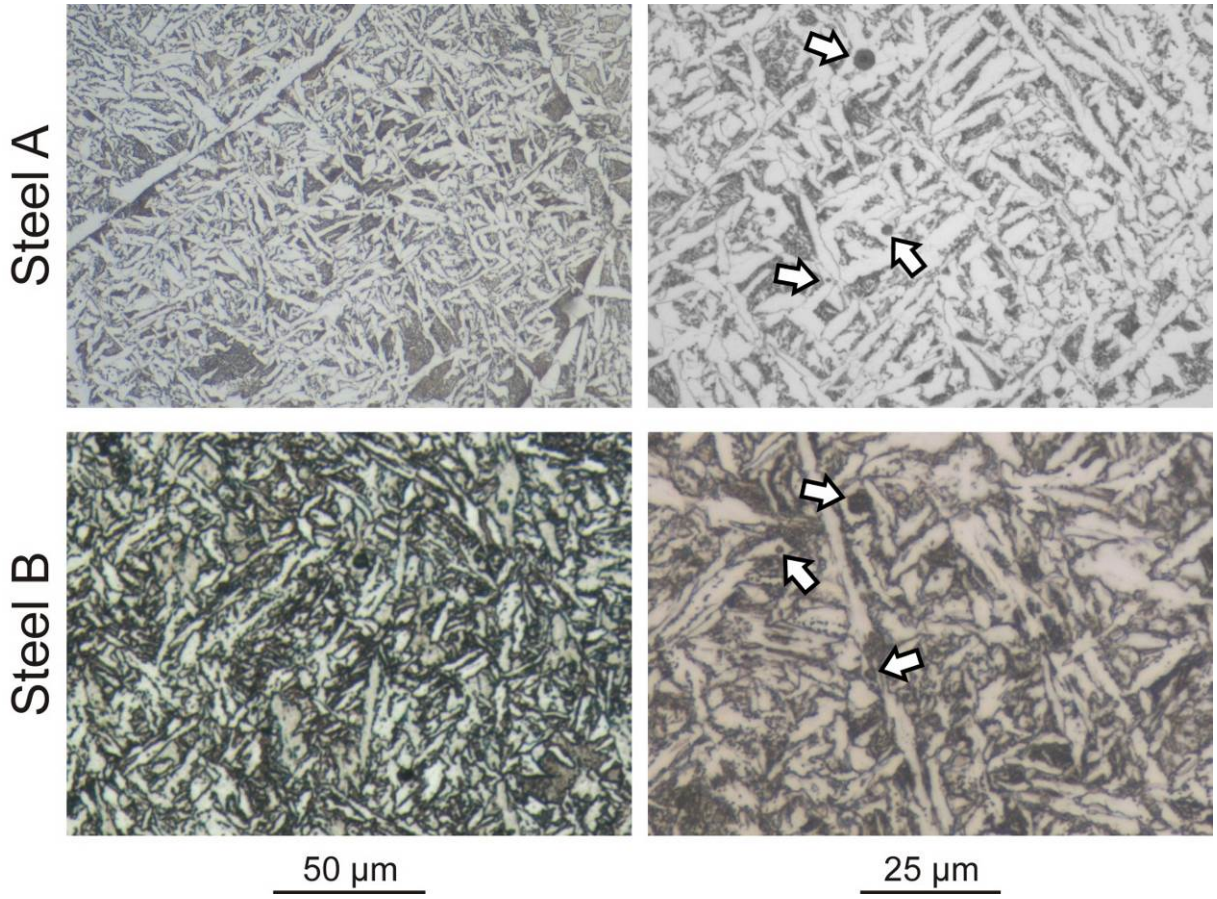


**Figure 8:** Final microstructure of steel A after heat treatment A-2 and steel B after heat treatment B-1.

In addition, the number of active inclusions is higher in steel A, as described in more detail in the following subsection. However, the experimental processing obviously also affects the capability of active inclusion types, so that with the same or an even lower number of particles a higher amount of acicular ferrite can be produced. This result also indicates the importance of the influencing factors' coaction. A possibly high percentage of acicular ferrite in the microstructure can only be achieved if all influencing factors are adjusted most favorable regarding a high potential for acicular ferrite formation.

### 3.3. Non-metallic inclusions

**Figure 9** shows the inclusion types determined by automated SEM/EDS analyses and by thermodynamic calculations using FactSage 6.4 for steel A:

- Steel A contains a huge amount of Ti-oxides, mostly in combination with Mn and/or Al. However, automated SEM/EDS analysis only displays the overall particle's composition, but do not provide information about its morphology. Therefore, it is hardly possible to differ between single- and multi-phase inclusions based on results of automated measurements. The thermodynamic

calculations predict a significant amount of ASlag, $TiO_x$ and $Al_2O_3$ inclusions. Due to the limitation of SEM/EDS, single-phase ASlag particles and multi-phase inclusions consisting of $TiO_x$ and $Al_2O_3$, which formed by heterogeneous nucleation, can both correspond to the mixed oxides detected by SEM/EDS.

- The measured and the calculated results indicate a substantial amount of MnS. Manual analyses show that MnS tends to nucleate heterogeneously on oxides, forming complex Ti-Mn- and Ti-Al-Mn-oxysulphides. However, this heterogeneous nucleation cannot be considered by the performed thermodynamic calculations.
- In addition, TiN and TiC are predicted by FactSage to be stable. A considerable amount of TiN and $(Ti,Mn)_xS_yN_z$ is detected in the final sample. As already explained, the distinction between single- and multi-phase particles is not possible by automated SEM/EDS analysis. But according to the inclusion types calculated by FactSage and the conducted manual inclusion characterizations, $(Ti,Mn)_xS_yN_z$ is suggested as heterogeneous type consisting of TiN and MnS. TiC is not found by SEM/EDS, which may be the caused by the small size of carbide precipitations (< 1.1 µm ECD), which is below the used detection limit of SEM/EDS. Additionally, the FactSage calculations display equilibrium conditions, which will never be reached in a practical experiment with defined cooling rate. Therefore, the results of SEM/EDS and FactSage may be quite well comparable at high temperatures, where the chemical driving force is high, but may differ significantly at lower temperatures. Hence, especially inclusion phases forming late in the cooling process will behave differently in the experiment than in the equilibrium calculation of FactSage.

In **Figure 10** the results regarding the inclusion landscape in steel B of the automated SEM/EDS analysis and of the thermodynamic calculations with FactSage are illustrated:

- The SEM/EDS results show that the main inclusion types in steel B are TiN and MnS.
- Only a very small number of oxides and oxysulfides is found in steel B. This is in agreement with the thermodynamic calculations, which also predict only a small amount of oxides. Although, also a high amount of TiN is predicted in steel A, comparing the ratio between TiN and oxides in steel A and B, shows that the frequency of oxides is much higher in steel A.
- The variations in the final inclusion landscapes may be explained by the different used processes in routes A and B. First, the control of conditions is more difficult in the large-scaled system of route B. Second, the longer holding time and stronger bath movements in route B can lead to a higher separation of oxide inclusions, which are already stable in the liquid melt. MnS and TiN, which form during solidification, are not strongly affected by this phenomenon. Hence, steel B shows a lower oxygen content, so that the amount of oxides is

decreased in favor of TiN. Third, the use of MgO-based refractories in route B instead of an alumina crucible reduced the amount of $Al_2O_3$-containing inclusions significantly. However, the number of MgO-containing inclusions is small compared to other types, so that they are included in the inclusion class 'Others'.

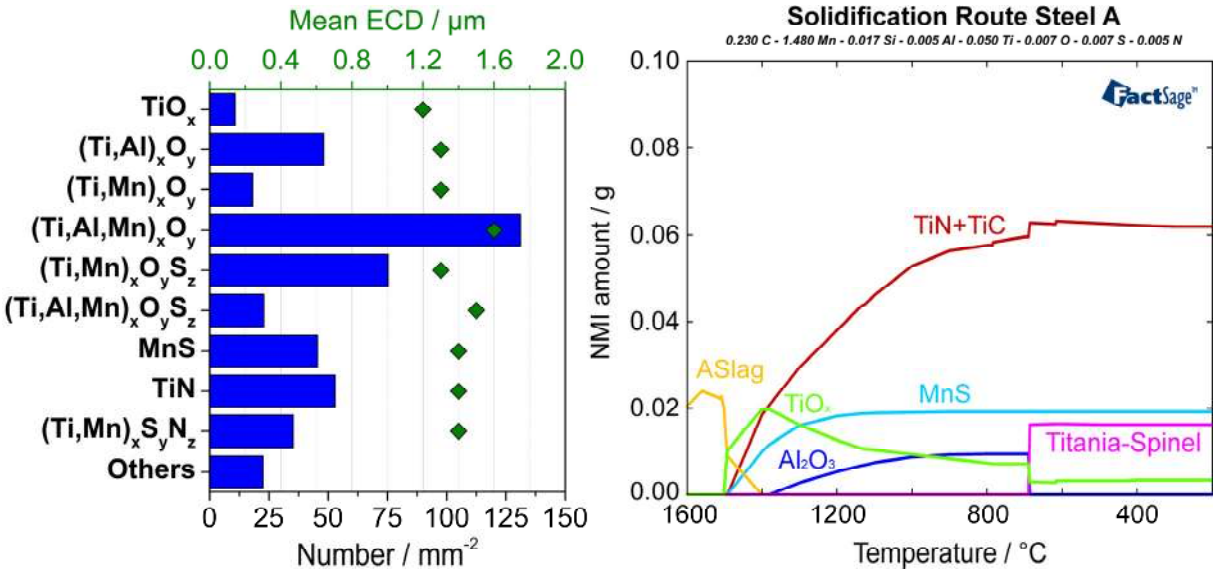


**Figure 9:** Inclusion landscape in steel A – SEM/EDS results compared with thermodynamic calculations.

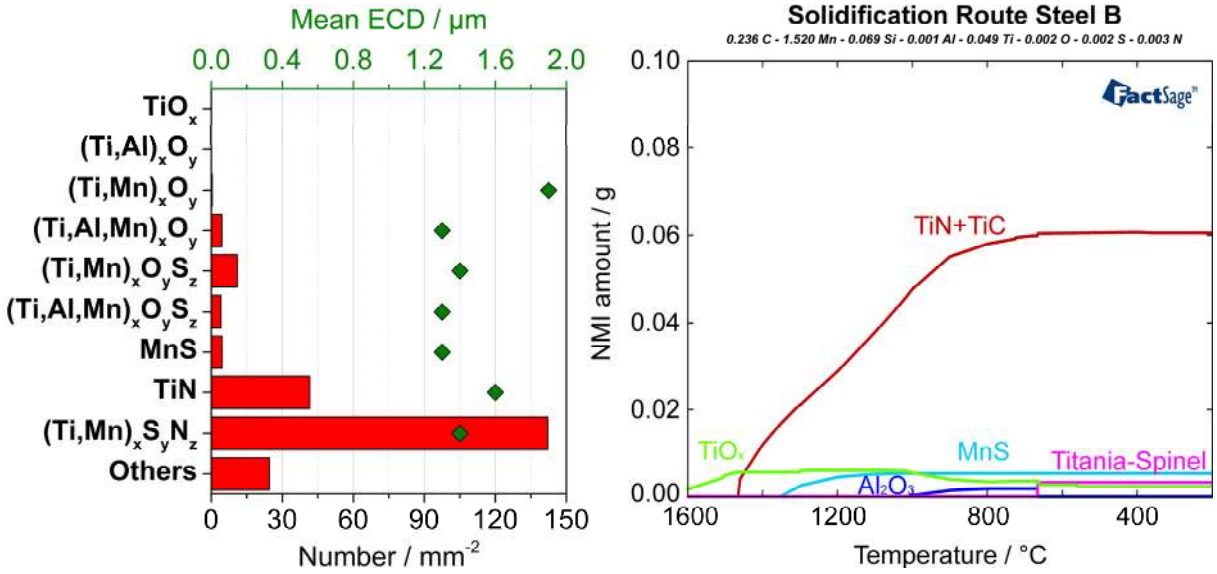


**Figure 10:** Inclusion landscape in steel B – SEM/EDS results compared with thermodynamic calculations.

The size of the detected inclusions is comparable in both steels. As it can be seen in **Figure 9** and **Figure 10** the mean ECD of the various inclusion classes is in both

steels between 1.2 and 1.6 µm. In addition, the inclusion size distributions, shown in **Figure 11**, are comparable. Barbaro et al.[36] suggested that especially the inclusion size influences inclusion's potential for acicular ferrite and suggested a minimum necessary particle size of 0.4 – 0.6 µm. The present work only studied inclusions above 1.1 µm; hence, the required particle size is reached for all inclusion classes. However, the present work showed that for inclusions above the minimum size, the influence of inclusion composition is of increasing importance. Inclusions with similar sizes provide different capabilities for acicular ferrite due to their chemical composition, e.g. MnS and TiN.

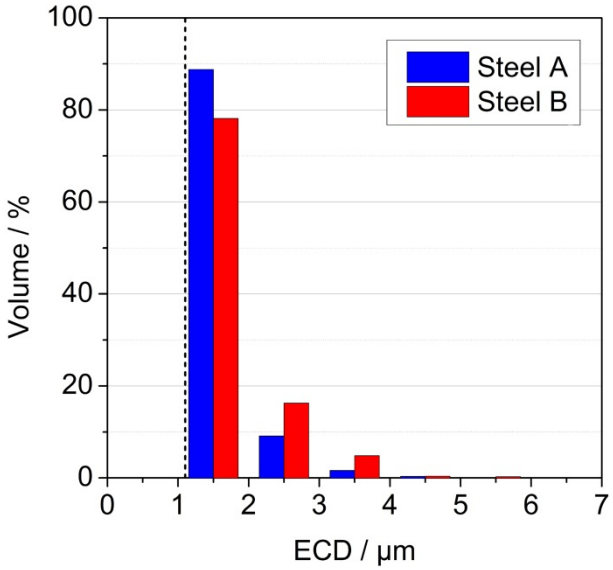


**Figure 11:** Distribution of inclusion size in steels A and B.

The potential of the detected inclusion classes to act as nuclei for acicular ferrite is determined by manual SEM/EDS analyses of active inclusions. The resulting percentage distributions for steel A and B are given in **Table 4**:

- In both steels pure $TiO_x$ and TiN are fond as completely inert.
- $(Ti,Al)_xO_y$ and $(Ti,Al,Mn)_xO_y$ are only found as acicular ferrite nuclei in steel A, what may be caused by the significantly lower contents of these inclusion types in steel B.
- $(Ti,Mn)_xO_y$ and $(Ti,Al,Mn)_xO_yS_z$ inclusions show a very high ability to act as nuclei for acicular ferrite in steel A and B. Although, only low to medium numbers of these inclusion classes are present in the steels, they belong to the major active types. A typical active $(Ti,Al,Mn)_xO_yS_z$ inclusion is illustrated in **Figure 12**.
- $(Ti,Mn)_xO_yS_y$ and MnS particles are identified as effective in both steels. Although, they are asserted as higher active in steel B than in steel A because their amount is lower in steel B, but they represent the same or even a larger share of the active inclusions in this steel.

- $(Ti,Mn)_xS_yN_z$ shows a very low capability for acicular ferrite. Steel A contains less $(Ti,Mn)_xS_yN_z$, so that the driving force for acicular ferrite is small to nucleate on this inclusion type. Contrary, steel B provides a huge amount of $(Ti,Mn)_xS_yN_z$ nucleation sites, so that occasionally acicular ferrite also nucleates on these inclusions.
- Generally, the capability of active inclusion types is higher in steel B and so steel B also provides a higher fraction of acicular ferrite in the microstructure, although the austenite grain size in steel B is smaller due to pinning effects by the high number of TiN particles. Hence, the processing obviously also influences inclusions' potential for acicular ferrite. However, the current results do not provide a complete explanation for this phenomenon. Further studies will be performed to clarify this effect.

**Table 4:** Active inclusion types in the steels A and B.

| | **Steel A - Share of … [%]** | | **Steel B - Share of … [%]** | |
|---|---|---|---|---|
| | Active inclusions | Total inclusions | Active inclusions | Total inclusions |
| **$TiO_x$** | 0,0 | 2,4 | 0,0 | 0,0 |
| **$(Ti,Al)_xO_y$** | 11,1 | 10,9 | 0,0 | 0,0 |
| **$(Ti,Mn)_xO_y$** | 11,1 | 4,1 | 17,6 | 0,2 |
| **$(Ti,Al,Mn)_xO_y$** | 16,7 | 29,8 | 0,0 | 2,2 |
| **$(Ti,Mn)_xO_yS_z$** | 8,3 | 17,1 | 47,1 | 5,3 |
| **$(Ti,Al,Mn)_xO_yS_z$** | 44,4 | 5,2 | 11,8 | 2,0 |
| **MnS** | 8,3 | 10,3 | 5,9 | 2,2 |
| **TiN** | 0,0 | 12,0 | 0,0 | 20,0 |
| **$(Ti,Mn)_xS_yN_z$** | 0,0 | 8,0 | 17,6 | 68,2 |

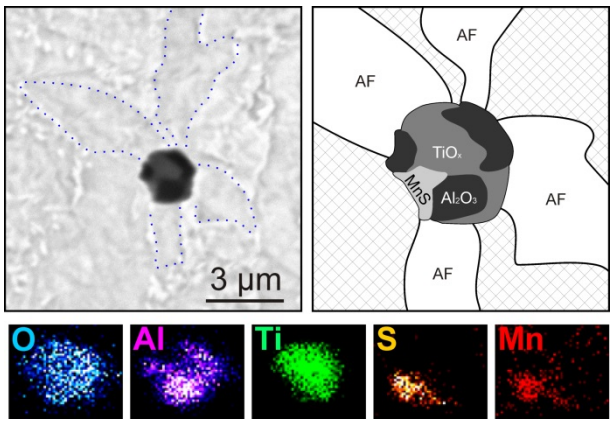


**Figure 12:** Non-metallic inclusion that acts as nucleus for acicular ferrite in steel A.

## 4. Conclusion

Due to the high toughness of acicular ferrite, steel properties can be significantly optimized by increasing the amount of acicular ferrite in the microstructure. The formation of acicular ferrite is mainly influenced by the steel composition, non-metallic inclusions, cooling rate and austenite grain size. These parameters interact strongly, so the systematic investigation of acicular ferrite formation is important. The present work describes two different laboratory approaches: a single-step route, using dipping tests in a vacuum induction furnace, and a two-step route, consisting of melting experiments in a Tammann type furnace and a subsequent heat treatment by HT-LSCM. The following conclusions can be drawn:

1. The formation of acicular ferrite is strongly influenced by the former processing. Favorable conditions for acicular ferrite formation differ between route A and route B, although the investigated steel composition is similar:
    a. The cooling rate influences the final amount of acicular ferrite essentially. The optimum cooling rate to obtain a possibly high acicular ferrite amount is different between route A and B and is strongly dependent on the prior processing of the sample. Applying comparable cooling rates in both routes leads to significant differences in the final acicular ferrite amount.
    b. Similar active inclusion types are found in steel A and B. Especially $(Ti,Mn)_xO_y$ and $(Ti,Al,Mn)_xO_yS_z$ inclusions are found as highly potent nucleation sites. Nevertheless, the capability of effective inclusions is also significantly influenced by the former processing.
    c. Although austenite grain size in steel A was significantly larger, the observed acicular ferrite amount in the final sample was higher in steel B than steel A when using the optimized cooling conditions in both cases. Thus, austenite grain size seems to only have a minor effect on the acicular ferrite formation in the present study.

2. Both experimental approaches are well suited for the examination of acicular ferrite formation on the laboratory scale, providing a systematic possibility for studying the related influence parameters. However, the advantages and limitations of both routes have to be considered:
    a. The steel composition can be adjusted and investigated in a satisfying way by both routes; although, it is easier to handle in route A because of the smaller system and better controllable conditions. Additionally, the smaller scale and the easy furnace handling of the Tammann type furnace experiment allow for a larger range of tested steel compositions.
    b. The influence of non-metallic inclusions can be analyzed by route A. The small system enables an accurate prediction of the formation of inclusions by thermodynamic calculations. Due to the two-step

methodology, a check of the inclusion landscape before heat treatment is possible. Route B is also a valuable tool, but because of the larger system, more disturbances affect the inclusion landscape.

c. The cooling rate is well controllable by HT-LSCM in route A. In route B, the cooling rate can only be varied by changing the dip time, which results in varying sample thicknesses and therefore different cooling rates of the sample.
d. The austenite grain size can be varied in the HT-LSCM experiment by austenitization temperature and time. In the dipping test, the austenite grain size can hardly be controlled.
e. The conditions in route B are more comparable to industrial practice than those in route A. Therefore, route B is more significant with respect to industrial feasibility and the related large-scale problems.

## Acknowledgement

Financial support by the Federal Ministry for Transport, Innovation and Technology (bmvit) and the Austrian Science Fund (FWF): [TRP 266-N19] as well as the Austrian Federal Government and the Styrian Provincial Government, represented by Österreichische Forschungsförderungsgesellschaft mbH and by Steirische Wirtschaftsförderungsgesellschaft mbH within the research activities of the K2 Competence Centre on “Integrated Research in Materials, Processing and Product Engineering”, operated by the Materials Center Leoben Forschung GmbH in the framework of the Austrian COMET Competence Centre Programme, is gratefully acknowledged.

## References

1. S. Ogibayashi: ‘Advances in technology of oxide metallurgy’, Nippon Steel Technical Report 61, Nippon Steel Corporation, Tokyo, Japan, 1994, 70–76.
2. H. K. D. H. Bhadeshia: ‘Modelling of steel welds’, *Mater. Sci. Technol.*, 1992, **8**, (2), 123–133.
3. C. van der Eijk, Ø. Grong and J. Hjelen: ‘Quantification of inclusion-stimulated ferrite nucleation in wrought steel using the SEM-EBSD technique’, Proc. Int. Conf. on ‘Solid-Solid Phase Transformations’, Kyoto, Japan, May 1999, JIM, 1573–1576.
4. H. K. D. H. Bhadeshia: ‘Bainite in steels: transformations, microstructure and properties’, 2nd edn, Chap. 10, ‘Acicular ferrite’, 237-276; 2001, London, IoM Communications.

5. Ø. Grong, A. O. Kluken, H. K. Nylund, A. L. Dons and J. Hjelen: ‘Catalyst effects in heterogeneous nucleation of acicular ferrite’, *Metall. Mater. Trans.*, 1995, **26A**, (3), 525–534.

6. D. S. Sarma, A. V. Karasev and P. G. Jönsson: ‘On the role of non-metallic inclusions in the nucleation of acicular ferrite in steels’, *ISIJ Int.*, 2009, **49**, (7), 1063–1074.

7. J. M. Gregg and H. K. D. H. Bhadeshia: ‘Solid-state nucleation of acicular ferrite on minerals added to molten steel’, *Acta Materialia*, 1997, **45**, (2), 739–748.

8. M. Andersson, J. Janis, L. Holappa, M. Kiviö, P. Naveau, M. Brandt, D. Espinosa, L. Bellavia, X. Vanden Eynde, E. de Courcy, L. Chapuis, T. Iung, S. Ekerot and C. van der Eijk: ‘Grain size control in steel by means of dispersed non-metallic inclusions’, Final report GRAINCONT EUR 24991, European Commission, Luxembourg, Luxembourg, 2011.

9. C. Xuan, W. Mu, P. G. Jönsson and K. Nakajima: ‘Effect of the Ti, Al contents on the inclusion characteristics in steels with $TiO_2$ and TiN particle additions’, Proc. 9th Int. Conf. on Clean Steel, Budapest, Hungary, Sept. 2015, OMBKE, 1–12.

10. C. Xuan, W. Mu, Z. I. Olano, P. G. Jönsson and K. Nakajima: ‘Effect of the Ti, Al contents on the inclusion characteristics in steels with $TiO_2$ and TiN particle additions’, *steel research int.*, 2015, DOI 10.1002/srin.201500267.

11. R. A. Farrar and P. L. Harrison: ‘Acicular ferrite in carbon-manganese weld metals: An overview’, *J. Mater. Sci.*, 1987, **22**, (11), 3812–3820.

12. R. A. Farrar, Z. Zhang, S. R. Bannister and G. S. Barritte: ‘The effect of prior austenite grain size on the transformation behaviour of C-Mn-Ni weld metal’, *J. Mater. Sci.*, 1993, **28**, (5), 1385–1390.

13. Z. Zhang and R. A. Farrar: ‘Role of non-metallic inclusions in formation of acicular ferrite in low alloy weld metals’, *Mater. Sci. Technol.*, 1996, **12**, (3), 237–260.

14. W. Mu, P. G. Jönsson and K. Nakajima: ‘Effect of Sulfur content on inclusion and microstructure characteristics in steels with $Ti_2O_3$ and $TiO_2$ additions’, *ISIJ Int.*, 2014, **54**, (12), 2907–2916.

15. M. N. Ilman, R. C. Cochrane and G. M. Evans: ‘The development of acicular ferrite in reheated Ti–B–Al–N type steel weld metals containing various levels of aluminium and nitrogen’, *Weld World*, 2015, **59**, (4), 565–575.

16. W. Mu, H. Mao, P. G. Jönsson and K. Nakajima: ‘Effect of carbon content on the potency of the intragranular ferrite formation’, *steel research int.*, 2015, DOI 10.1002/srin.201500043.

17. X. Wan, K. Wu, L. Cheng and R. Wei: ‘In-situ observations of acicular ferrite growth behavior in the simulated coarse-grained heat-affected zone of high-strength low-alloy steels’, *ISIJ Int.*, 2015, **55**, (3), 679–685.

18. R. A. Ricks, P. R. Howell and G. S. Barritte: ‘The nature of acicular ferrite in HSLA steel weld metals’, *J. Mater. Sci.*, 1982, **17**, (3), 732–740.

19. M.-M. Song, B. Song, C.-L. Hu, W.-B. Xin and G.-Y. Song: ‘Formation of acicular ferrite in Mg treated Ti-bearing C–Mn steel’, *ISIJ Int.*, 2015, **55**, (7), 1468–1473.

20. D. Loder and S. K. Michelic: ‘Specific use of non-metallic inclusions for the formation of acicular ferrite structures: thermodynamic modeling and laboratory experiments’, Proc. 9th Int. Conf. on Clean Steel, Budapest, Hungary, Sept. 2015, OMBKE, 1–12.

21. J. Wiener: ‘Sekundärmetallurgische Aspekte der Herstellung hoch manganhaltiger Stähle’, PhD thesis, Montanuniversitaet Leoben, Leoben, Austria, 2010, 95-98.

22. S. K. Michelic, M. Hartl and B. Christian: ‘Thermodynamic and experimental study on the modification of nonmetallic inclusions through the contact with CaO-$Al_2O_3$-MgO slags’, Proc. Conf. AISTech Vol. II, Indianapolis, Indiana, USA, May 2011, AIST, 618–626.

23. C. Bernhard, S. Schider, A. Sormann, G. Xia and S. Ilie: ‘Erste Ergebnisse des neuen Hochtemperatur-Konfokalmikroskops am Lehrstuhl für Metallurgie’, *BHM*, 2011, **156**, (5), 161–167.

24. P. Presoly, R. Pierer and C. Bernhard: ‘Linking up of HT-LSCM and DSC measurements to characterize phase diagrams of steels’, *IOP Conf. Ser.: Mater. Sci. Eng.*, 2012, **33**, 1–9.

25. P. Presoly, R. Pierer and C. Bernhard: ‘Identification of defect prone peritectic steel grades by analyzing high-temperature phase transformations’, *Metall. Mater. Trans.*, 2013, **44A**, (12), 5377–5388.

26. S. Michelic, J. Goriupp, S. Feichtinger, Y.-B. Kang, C. Bernhard and J. Schenk: ‘Study on oxide inclusion dissolution in secondary steelmaking slags using high temperature confocal scanning laser microscopy’, *steel research int.*, 2016, **87**, (1), 57-67.

27. D. Loder, S. K. Michelic, A. Mayerhofer, C. Bernhard and R. J. Dippenaar: ‘In situ observation of acicular ferrite formation using HT-LSCM: possibilities, challenges and influencing factors’, Proc. MS&T Conf., Pittsburgh, Pennsylvania, USA, Oct. 2014, ASM Int., 469–476.

28. B. Linzer, C. Bernhard and G. Hohenbichler: ‘Experimentelle Simulation der Mikrostruktur von gegossenen Dünnbändern’, *BHM*, 2004, **149**, (3), 107–111.

29. B. Linzer, G. Hohenbichler, S. Bragin, G. Arth and C. Bernhard: ‘Experimental simulation of the solidification of steel at higher cooling rates’, *BHM*, 2009, **154**, (11), 498–503.

30. W. Vanovsek, C. Bernhard, M. Fiedler and R. Schnitzer: ‘Effect of titanium on the solidification and postsolidification microstructure of high-strength steel welds’, *Weld World*, 2013, **57**, (5), 665-674.

31. S. K. Michelic, D. Loder, G. Arth and C. Bernhard: ‘Experimental study on the formation of non-metallic inclusions acting as nuclei for acicular ferrite in HSLA steels through specific deoxidation practice and defined cooling conditions’, *Mater. Sci. Forum*, 2014, **783-786**, 1079–1084.

32. D. Loder, S. K. Michelic and C. Bernhard: ‘Characterization of acicular ferrite microstructures using etching methods, optical microscopy and HT-LSCM’, Proc. 14th Metallography Conf., Leoben, Austria, Sept. 2014, Montanuniversitaet Leoben, 1-6.

33. M. Nuspl, W. Wegscheider, J. Angeli, W. Posch and M. Mayr: ‘Qualitative and quantitative determination of micro-inclusions by automated SEM/EDX analysis’, *Anal. Bioanal. Chem.*, 2004, **379**, (4), 640–645.

34. S. K. Michelic, G. Wieser and C. Bernhard: ‘On the representativeness of automated SEM/EDS analyses for inclusion characterisation with special regard to the measured sample area’, *ISIJ Int.*, 2011, **51**, (5), 769–775.

35. S. K. Michelic, D. Loder, T. Reip, A. Ardehali Barani and C. Bernhard: ‘Characterization of TiN, TiC and Ti(C,N) in titanium-alloyed ferritic chromium steels focusing on the significance of different particle morphologies’, *Mater. Charact.*, 2015, **100**, 61–67.

36. F. J. Barbaro, P. Krauklis and K. E. Easterling: ‘Formation of acicular ferrite at oxide particles in steels’, *Mater. Sci. Technol.*, 1989, **5**, (11), 1057-1068.

**Content of tables:**



**Content of figures:**